EPJ Web of Conferences **3**, 01003 (2010)
DOI:10.1051/epjconf/20100301003

Coulomb Effects in Few-Body Reactions

A. Deltuva[a]

Centro de Física Nuclear da Universidade de Lisboa, P-1649-003 Lisboa, Portugal

Abstract. The method of screening and renormalization is used to include the Coulomb interaction between the charged particles in the momentum-space description of three- and four-body nuclear reactions. The necessity for the renormalization of the scattering amplitudes and the reliability of the method is demonstrated. The Coulomb effect on observables is discussed.

1 Introduction

The inclusion of the long-range Coulomb interaction in the description of the three- and four-particle scattering is a challenging task in theoretical few-body nuclear physics. The long range of the Coulomb potential prevents the direct application of the standard scattering theory. There is a number of suggestions how to overcome this difficulty; most of them are based on the configuration-spac framework [1–4] and are limited to energies below three-body breakup threshold, while the others [5–8] have not matured yet into practical applications. Up to now only few approaches led to the results above three-body breakup threshold. Those are configuration-spac calculations for proton-deuteron (p-d) elastic scattering using the Kohn variational principle [9] and the screening and renormalization method in the framework of momentum-space integral equations [10–13]; the latter approach will be discussed here in more details. Very recently p-d results above three-body breakup threshold were also obtained using modifie Faddeev equation in configuratio space together with the dumping of particular Coulomb contributions [14].

2 Method of screening and renormalization

In nature the Coulomb potential w_C is always screened at large distances. The comparison of the data from typical nuclear physics experiments and theoretical predictions with full Coulomb is meaningfull only if the full and screened Coulomb become *physically indistinguishable*. This was proved in Refs. [15, 16] where the screening and renormalization method for the scattering of two charged particles was proposed. We base our treatment of the Coulomb interaction on that idea.

The standard scattering theory is formally applicable to the screened Coulomb potential w_R, i.e., the Lippmann-Schwinger equation yields the two-particle transition matrix

$$t_R = w_R + w_R g_0 t_R \tag{1}$$

where g_0 is the free resolvent. In the configuration-spac representation we choose the screened Coulomb potential as

$$w_R(r) = w_C(r)\, e^{-(r/R)^n} \tag{2}$$

with R being the screening radius and n controlling the smoothness of the screening. It was proven in Ref. [15] that in the limit of infinit screening radius R the on-shell screened Coulomb transition matrix (screened Coulomb scattering amplitude) $\langle \mathbf{p}'|t_R|\mathbf{p}\rangle$ with $p' = p$, renormalized by the infinitel oscillating phase factor $z_R^{-1}(p) = e^{2i\phi_R(p)}$, approaches the full Coulomb amplitude $\langle \mathbf{p}'|t_C|\mathbf{p}\rangle$ in general *as a distribution*, i.e.,

$$\lim_{R\to\infty} z_R^{-1}(p) \int d^2\hat{\mathbf{p}} \langle \mathbf{p}'|t_R|\mathbf{p}\rangle \varphi(\hat{\mathbf{p}}) = \int d^2\hat{\mathbf{p}} \langle \mathbf{p}'|t_C|\mathbf{p}\rangle \varphi(\hat{\mathbf{p}}) \tag{3}$$

for any test function $\varphi(\hat{\mathbf{p}})$ with the properties given in Ref. [15]; in particular, it must vanish for forward scattering, i.e., $\varphi(\hat{\mathbf{p}}') = 0$. Reference [15] uses partial wave expansion, which for the full Coulomb amplitude itself converges only as a distribution, and it therefore is unable to make any conclusions on the possible pointwise convergence. However, as argued already in Ref. [15], the convergence of the renormalized screened Coulomb scattering amplitude to the full Coulomb amplitude in the sense of distributions is sufficient for the description of physical observables. For a fi ed fina state observation direction $\hat{\mathbf{p}}'$ the cross section is determined not directly by the scattering amplitude, but by the outgoing wave packet

$$\varphi_f(\mathbf{p}') = \int d^3\mathbf{p} \langle \mathbf{p}'|S|\mathbf{p}\rangle \varphi_i(\mathbf{p}) \tag{4}$$

$$\sim \int d^2\hat{\mathbf{p}} \langle \mathbf{p}'|t_R|\mathbf{p}\rangle \varphi_i(\mathbf{p})|_{p=p'} \tag{5}$$

that is related to the initial wave packet $\varphi_i(\mathbf{p})$ by the S-matrix or the scattering amplitude. Thus, in the step from the scattering amplitude to the cross section one has to go through the conceptual exercise of averaging the scattering

[a] e-mail: deltuva@cii.fc.ul.pt

amplitude over the initial state physical wave packet being peaked around the experimental beam momentum $\mathbf{p}_i$. Thus, on the rhs of Eq. (3) $\langle \mathbf{p}'|t_C|\mathbf{p}_i\rangle$ itself is picked out in that average. In addition, the outgoing wave packet is never observed in the forward direction, i.e., $\hat{\mathbf{p}}' \neq \hat{\mathbf{p}}_i$; the necessary property $\varphi_i(\mathbf{p}') = 0$ can therefore always be fulfille by the sharpness of the initial wave packet. In the practical calculations [11,12] the above averaging is carried out implicitly, replacing the renormalized screened Coulomb amplitude in the $R \to \infty$ limit by the full one, i.e.,

$$\lim_{R\to\infty} z_R^{-1}(p)\langle \mathbf{p}'|t_R|\mathbf{p}\rangle \to \langle \mathbf{p}'|t_C|\mathbf{p}\rangle. \tag{6}$$

Since $z_R^{-1}(p)$ is only a phase factor, the above relations indeed demonstrate that the physical observables become insensitive to screening provided it takes place at sufficiently large distances R and, in the $R \to \infty$ limit, coincide with the corresponding quantities referring to the full Coulomb. Furthermore, renormalization by $z_R^{-\frac{1}{2}}(p_i)$ in the $R \to \infty$ limit relates also the screened and full Coulomb wave functions [17], i.e.,

$$\lim_{R\to\infty} (1 + g_0 t_R)|\mathbf{p}\rangle z_R^{-\frac{1}{2}}(p) = |\psi_C^{(+)}(\mathbf{p})\rangle. \tag{7}$$

2.1 Three-particle scattering

The screening and renormalization method based on the above relations can be extended to more complicated systems, albeit with some limitations. The systems of two- and three-particles interacting via pairwise strong short-range and screened Coulomb potentials, v_α and $w_{\alpha R}$, $\alpha = 1,2,3$, is considered in Refs. [12,13,18]. Here we extend our treatment to a more general case where an irreducible three-body force

$$V_{(3)} = \sum_{\alpha=1}^{3} u_\alpha \tag{8}$$

is present; it is decomposed into three terms u_α. The full resolvent

$$G^{(R)} = [E + i0 - H_0 - \sum_\gamma (v_\gamma + u_\gamma + w_{\gamma R})]^{-1}, \tag{9}$$

with H_0 being the three-particle kinetic energy operator and E the available energy may be decomposed into channel resolvents

$$G_\alpha^{(R)} = (E + i0 - H_0 - v_\alpha - w_{\alpha R})^{-1}, \tag{10}$$

and the multichannel three-particle transition operator $U_{\beta\alpha}^{(R)}$ according to

$$G^{(R)} = \delta_{\beta\alpha} G_\alpha^{(R)} + G_\beta^{(R)} U_{\beta\alpha}^{(R)} G_\alpha^{(R)}; \tag{11}$$

all operators depend parametrically on the Coulomb screening radius R. The full multichannel transition matrix $U_{\beta\alpha}^{(R)}$ for elastic and rearrangement scattering is calculated from the integral equation [19]

$$\begin{aligned} U_{\beta\alpha}^{(R)} = {} & \bar{\delta}_{\beta\alpha} G_0^{-1} + \sum_\gamma \bar{\delta}_{\beta\gamma} T_\gamma^{(R)} G_0 U_{\gamma\alpha}^{(R)} \\ & + u_\alpha + \sum_\gamma u_\gamma G_0 (1 + T_\gamma^{(R)} G_0) U_{\gamma\alpha}^{(R)} \end{aligned} \tag{12}$$

that is a generalisation of the Alt, Grassberger, and Sandhas (AGS) equation [20] in the presence of the three-body force. $G_0 = (E + i0 - H_0)^{-1}$ is the free resolvent, $\delta_{\beta\alpha} = 1 - \delta_{\beta\alpha}$, and the two-particle transition matrix is derived from the full channel interaction $v_\alpha + w_{\alpha R}$, i.e.,

$$T_\alpha^{(R)} = (v_\alpha + w_{\alpha R}) + (v_\alpha + w_{\alpha R}) G_0 T_\alpha^{(R)}. \tag{13}$$

The on-shell matrix elements $\langle b_\beta \mathbf{q}'|U_{\beta\alpha}^{(R)}|b_\alpha \mathbf{q}\rangle$ are amplitudes (up to a factor) for elastic ($\beta = \alpha$) and rearrangement ($\beta \neq \alpha$) scattering. The channel states $|b_\alpha \mathbf{q}\rangle$ are the eigenstates of the corresponding channel Hamiltonian $H_\alpha = H_0 + v_\alpha$ with the energy eigenvalue E. $|b_\alpha \mathbf{q}\rangle$ is a product of the bound state wave function $|b_\alpha\rangle$ for the pair α and the plane wave with the relative particle-pair α momentum $\mathbf{q}$; the dependence on the discrete quantum numbers is suppressed in our notation.

In order to isolate the screened Coulomb contributions to the transition amplitude that diverge in the infinit R limit, we use a decomposition of the full resolvent into alternative channel resolvents

$$G_{\alpha R} = (E + i0 - H_0 - v_\alpha - w_{\alpha R} - W_{\alpha R}^{\text{c.m.}})^{-1}, \tag{14}$$

where $W_{\alpha R}^{\text{c.m.}}$ is the screened Coulomb potential between the spectator particle α and the center of mass (c.m.) of the remaining pair. The same screening function is used for both Coulomb potentials $w_{\alpha R}$ and $W_{\alpha R}^{\text{c.m.}}$. The corresponding transition matrix

$$T_{\alpha R}^{\text{c.m.}} = W_{\alpha R}^{\text{c.m.}} + W_{\alpha R}^{\text{c.m.}} G_\alpha^{(R)} T_{\alpha R}^{\text{c.m.}}, \tag{15}$$

is a two-body operator and therefore its on-shell and half-shell behaviour in the limit $R \to \infty$ is given by Eqs. (3) and (7). It relates the channel resolvents as

$$G_{\alpha R} = G_\alpha^{(R)} + G_\alpha^{(R)} T_{\alpha R}^{\text{c.m.}} G_\alpha^{(R)}. \tag{16}$$

Thus, the full resolvent can alternatively be decomposed into

$$G^{(R)} = \delta_{\beta\alpha} G_{\alpha R} + G_{\beta R} \tilde{U}_{\beta\alpha}^{(R)} G_{\alpha R} \tag{17}$$

$$\begin{aligned} = {} & \delta_{\beta\alpha} G_\alpha^{(R)} + G_\beta^{(R)} \delta_{\beta\alpha} T_{\alpha R}^{\text{c.m.}} G_\alpha^{(R)} \\ & + G_\beta^{(R)} [1 + T_{\beta R}^{\text{c.m.}} G_\beta^{(R)}] \tilde{U}_{\beta\alpha}^{(R)} [1 + G_\alpha^{(R)} T_{\alpha R}^{\text{c.m.}}] G_\alpha^{(R)}, \end{aligned} \tag{18}$$

where the reduced transition operator $\tilde{U}_{\beta\alpha}^{(R)}(Z)$ may be calculated through the integral equation

$$\begin{aligned} \tilde{U}_{\beta\alpha}^{(R)} = {} & \bar{\delta}_{\beta\alpha} (G_{\alpha R}^{-1} + v_\alpha) + u_\alpha + \delta_{\beta\alpha} \mathcal{W}_{\alpha R} \\ & + \sum_\gamma (\bar{\delta}_{\beta\gamma} v_\gamma + u_\gamma + \delta_{\beta\gamma} \mathcal{W}_{\beta R}) G_{\gamma R} \tilde{U}_{\gamma\alpha}^{(R)} \end{aligned} \tag{19}$$

which is driven by the strong two- and three-body potentials $\underline{v}_\alpha$ and u_α and the potential of three-body nature $\mathcal{W}_{\alpha R} = \sum_\gamma(\delta_{\alpha\gamma}w_{\gamma R} - \delta_{\alpha\gamma}W^{\rm c.m.}_{\gamma R})$. This potential $\mathcal{W}_{\alpha R}$ accounts for the difference between the direct Coulomb interaction $w_{\gamma R}$ and the auxiliary one $W^{\rm c.m.}_{\gamma R}$ that takes place between the charged particle and the c.m. of the remaining pair. When calculated between on-shell screened Coulomb states, $\tilde{U}^{(R)}_{\beta\alpha}$ is of short-range, even in the infinit R limit. Equation (17), together with Eq. (11), gives a relation between full and reduced three-particle transition operators, i.e.,

$$U^{(R)}_{\beta\alpha} = \delta_{\beta\alpha}T^{\rm c.m.}_{\alpha R} + [1 + T^{\rm c.m.}_{\beta R}G^{(R)}_\beta]\tilde{U}^{(R)}_{\beta\alpha}[1 + G^{(R)}_\alpha T^{\rm c.m.}_{\alpha R}] \quad (20)$$

$$= \delta_{\beta\alpha}T^{\rm c.m.}_{\alpha R} + (U^{(R)}_{\beta\alpha} - \delta_{\beta\alpha}T^{\rm c.m.}_{\alpha R}). \quad (21)$$

Thus, the three-particle transition operator $U^{(R)}_{\beta\alpha}$ has a long-range part $\delta_{\beta\alpha}T^{\rm c.m.}_{\alpha R}$ whereas the remainder $U^{(R)}_{\beta\alpha} - \delta_{\beta\alpha}T^{\rm c.m.}_{\alpha R}$ is a short-range operator that is externally distorted due to the screened Coulomb waves generated by $[1 + G^{(R)}_\alpha T^{\rm c.m.}_{\alpha R}]$. On-shell, both parts do not have a proper limit as $R \to \infty$ but the limit exists after renormalization by an appropriate phase factor, yielding the transition amplitude for full Coulomb

$$\langle b_\beta \mathbf{q}'|U^{(C)}_{\beta\alpha}|b_\alpha\mathbf{q}\rangle = \delta_{\beta\alpha}\langle b_\alpha\mathbf{q}'|T^{\rm c.m.}_{\alpha C}|b_\alpha\mathbf{q}\rangle$$
$$+ \lim_{R\to\infty}[Z^{-\frac{1}{2}}_{\beta R}(q')\langle b_\beta\mathbf{q}'|(U^{(R)}_{\beta\alpha} - \delta_{\beta\alpha}T^{\rm c.m.}_{\alpha R})|b_\alpha\mathbf{q}\rangle Z^{-\frac{1}{2}}_{\alpha R}(q)]. \quad (22)$$

The firs term on the right-hand side of Eq. (22) is known analytically [15]; it corresponds to the particle-pair α full Coulomb transition amplitude that results from the implicit renormalization of $T^{\rm c.m.}_{\alpha R}$ according to Eq. (6). The $R \to \infty$ limit for the remaining part $(U^{(R)}_{\beta\alpha} - \delta_{\beta\alpha}T^{\rm c.m.}_{\alpha R})$ of the multichannel transition matrix is performed numerically; due to the short-range nature of this term, as demonstrated in Eq. (20), the convergence with the increasing screening radius R is fast and the limit is reached with sufficient accuracy at finit R; furthermore, it can be calculated using the partial-wave expansion. We emphasize that Eq. (22) is by no means an approximation since it is based on the obviously exact identity (21) where the $R \to \infty$ limit for each term exists and is calculated separately.

The renormalization factor for $R \to \infty$ is a diverging phase factor

$$Z_{\alpha R}(q) = e^{-2i\Phi_{\alpha R}(q)}, \quad (23)$$

where $\Phi_{\alpha R}(q)$, though independent of the particle-pair relative angular momentum l in the infinit R limit, may be realized by

$$\Phi_{\alpha R}(q) = \sigma^\alpha_l(q) - \eta^\alpha_{lR}(q), \quad (24)$$

with the diverging screened Coulomb phase shift $\eta_{lR}(q)$ corresponding to standard boundary conditions and the proper Coulomb one $\sigma_l(q)$ referring to the logarithmically distorted proper Coulomb boundary conditions. For the screened Coulomb potential of Eq. (2) the infinit R limit of $\Phi_{\alpha R}(q)$ is known analytically,

$$\Phi_{\alpha R}(q) = \mathcal{K}_\alpha(q)[\ln(2qR) - C/n], \quad (25)$$

where $C \approx 0.5772156649$ is the Euler number and $\mathcal{K}_\alpha(q)$ is the Coulomb parameter. The form of the renormalization phase $\Phi_{\alpha R}(q)$ to be used in the actual calculations with finit screening radii R is not unique, but the converged results show independence of the chosen form of $\Phi_{\alpha R}(q)$.

For breakup observables we follow a very similar strategy where the starting point is the AGS-like equation for the breakup operator

$$U^{(R)}_{0\alpha} = G^{-1}_0 + \sum_\gamma T^{(R)}_\gamma G_0 U^{(R)}_{\gamma\alpha}$$
$$+ u_\alpha + \sum_\gamma u_\gamma G_0(1 + T^{(R)}_\gamma G_0)U^{(R)}_{\gamma\alpha} \quad (26)$$

and its relation to the full resolvent, i.e.,

$$G^{(R)} = G_0 U^{(R)}_{0\alpha} G^{(R)}_\alpha. \quad (27)$$

In the same spirit, we introduce auxiliary Coulomb resolvent

$$G_R = (E + i0 - H_0 - \sum_\gamma w_{\gamma R})^{-1}. \quad (28)$$

that keeps only the screened Coulomb interaction. The proper three-body Coulomb wave function and its relation to the three-body screened Coulomb wave function generated by G_R is, in general, unknown. This prevents the application of the screening and renormalization method to the reactions involving three free charged particles (nucleons or nuclei) in the fina state.

However, in the system of two charged particles and a neutral one, only the channel $\gamma = \rho$, corresponding to the correlated pair of charged particles, contributes to G_R which simplifie to

$$G_R = G_0 + G_0 T_{\rho R} G_0, \quad (29)$$

$$T_{\rho R} = w_{\rho R} + w_{\rho R} G_0 T_{\rho R}, \quad (30)$$

making channel ρ the most convenient choice for the description of the fina breakup state. Thus, for the purpose of breakup, a decomposition of the full resolvent, alternative to Eq. (27) is

$$G^{(R)} = G_R \tilde{U}^{(R)}_{0\alpha} G_{\alpha R} \quad (31)$$

$$= G_0[1 + T_{\rho R}G_0]\tilde{U}^{(R)}_{0\alpha}[1 + G^{(R)}_\alpha T^{\rm c.m.}_{\alpha R}]G^{(R)}_\alpha, \quad (32)$$

where the reduced breakup operator $\tilde{U}^{(R)}_{0\alpha}$ may be calculated through quadrature

$$\tilde{U}^{(R)}_{0\alpha} = G^{-1}_{\alpha R} + v_\alpha + u_\alpha + \sum_\gamma (v_\gamma + u_\gamma)G_{\gamma R}\tilde{U}^{(R)}_{\gamma\alpha}, \quad (33)$$

from the corresponding reduced operator $\tilde{U}^{(R)}_{\beta\alpha}(Z)$ of elastic/rearrangement scattering. On-shell, the reduced operator $\tilde{U}^{(R)}_{0\alpha}(Z)$ calculated between screened Coulomb distorted initial and fina states is of finit range, though the two contributions in Eq. (33) have slightly different range properties as discussed in Ref. [13]. The relation between the full and reduced breakup operators is

$$U^{(R)}_{0\alpha} = (1 + T_{\rho R}G_0)\tilde{U}^{(R)}_{0\alpha}(1 + G^{(R)}_\alpha T^{\rm c.m.}_{\alpha R}). \quad (34)$$

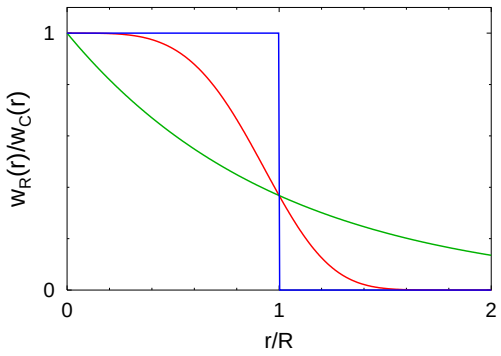

Fig. 1. Screening function $w_R(r)/w_C(r)$ as function of the distance r between charged particles for characteristic values of the parameter n in Eq. (2): $n = 1$ (green curve) corresponds to Yukawa screening, $n = 4$ (red curve) is our standard choice, and $n \to \infty$ (blue curve) corresponds to a sharp cutoff.

In the full breakup operator $U^{(R)}_{0\alpha}(Z)$ the external distortions show up in screened Coulomb waves generated by $(1 + G^{(R)}_{\alpha} T^{\rm c.m.}_{\alpha R})$ in the initial state and by $(1 + T_{\rho R} G_0)$ in the fina state; both wave functions do not have proper limits as $R \to \infty$. Therefore the full breakup transition amplitude in the case of the unscreened Coulomb potential is obtained via the renormalization of the on-shell breakup transition matrix $U^{(R)}_{0\alpha}$ in the infinit R limit

$$\langle \mathbf{p}'\mathbf{q}'|U^{(C)}_{0\alpha}|b_\alpha \mathbf{q}\rangle = \lim_{R\to\infty} [z_R^{-\frac{1}{2}}(p')\langle \mathbf{p}'\mathbf{q}'|U^{(R)}_{0\alpha}|b_\alpha \mathbf{q}\rangle Z^{-\frac{1}{2}}_{\alpha R}(q)], \tag{35}$$

where $\mathbf{p}'$ is the relative momentum between the charged particles in the fina state, $\mathbf{q}'$ the corresponding particle-pair relative momentum, and

$$z_R(p') = e^{-2i\kappa(p')[\ln(2pR) - C/n]} \tag{36}$$

the final-stat renormalization factor. The limit in Eq. (35) has to be performed numerically, but, due to the short-range nature of the breakup operator, the convergence with the increasing screening radius R is fast and the limit is reached with sufficient accuracy at finit R.

2.2 Practical realization

To calculate the short-range part of the elastic, rearrangement, and breakup scattering amplitudes (22) and (35) we solve standard scattering equations (12), (15), and (26) at finit Coulomb screening radius R using the momentum-space partial-wave representation as described in detail in Refs. [21–23]. We have to make sure that R is large enough to achieve (after renormalization) the R-independence of the results up to a desired accuracy. However, those R values are larger than the range of the nuclear interaction resulting in a slower convergence of the partial-wave expansion. As we found in Ref. [12], the practical success of the screening and renormalization method depends strongly on the choice of the screening function, i.e., on the choice of the exponent n in Eq. (2). One of the essential differences

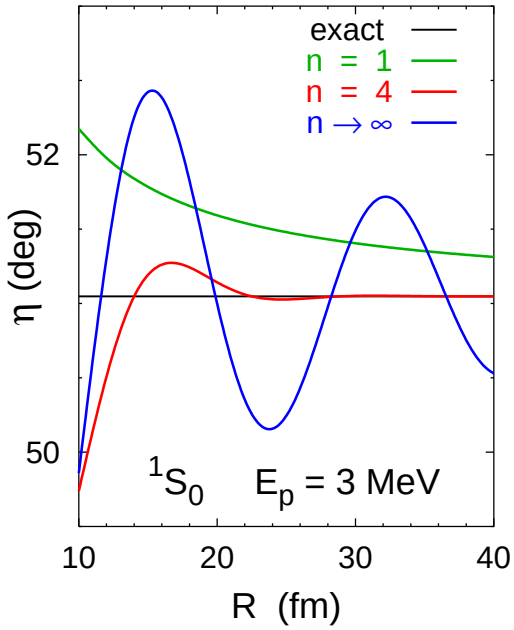

Fig. 2. Convergence of the $^1S_0$ pp phase shift η with screening radius R for 3 MeV proton lab energy. Results obtained with $n = 1$ (green curve), $n = 4$ (red curve), and $n \to \infty$ (blue curve) screening functions are compared with exact value given by black line.

compared to previous works [10,11,24,25] is that we use a sharper screening than the Yukawa screening ($n = 1$). We want to ensure that the screened Coulomb potential w_R approximates well the true Coulomb one w_C for distances $r < R$ and simultaneously vanishes rapidly for $r > R$, providing a comparatively fast convergence of the partial-wave expansion. However, the sharp cutoff ($n \to \infty$) yields an unpleasant oscillatory behavior in the momentum-space representation, leading to convergence problems. We fin values $3 \le n \le 8$ to provide a sufficiently smooth, but at the same time a sufficiently rapid screening around $r = R$. The screening functions for different n values are compared in Fig. 1, showing that the present choice $n = 4$ includes much more of the exact Coulomb potential at short distances than the Yukawa screening used previously. For example, Yukawa screening requires a screening radius of $R = 1280$ fm in order to approximate true Coulomb at relative distance $r = 5$ fm as well as the present choice does with $R = 20$ fm. As shown in Fig. 2 for the proton-proton (pp) $^1S_0$ phase shift, the convergence with the screening radius for $n = 4$ is much faster than for Yukawa screening or sharp cutoff. Furthermore, due to the much shorter range of the $n = 4$ screening compared to the Yukawa screening, the quasisingularities of the screened Coulomb potential are far less pronounced in the $n = 4$ case. With our optimal choice $3 \le n \le 8$ the convergence of the partial-wave expansion, though being slower than for the nuclear interaction alone, can still be achieved; alternatively, a perturbative approach for higher two-particle partial waves [26] that is computationally less demanding but, nevertheless, highly reliable as proved in Ref. [27], can be used as well.

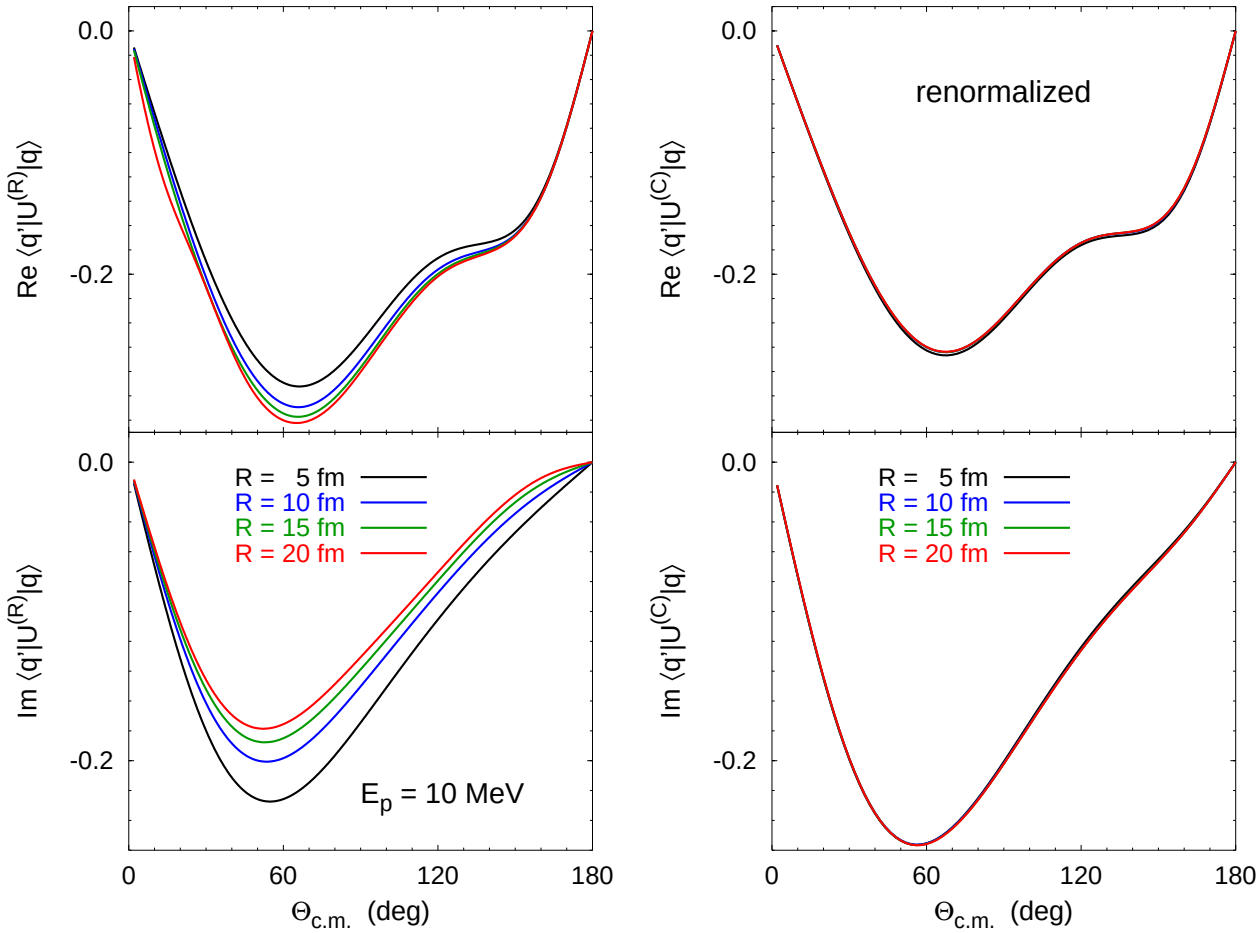

Fig. 3. Real and imaginary parts of nonrenormalized (left side) and renormalized (right side) *p-d* elastic scattering amplitudes (in arbitrary units) at $E_p = 10$ MeV shown as functions of the c.m. scattering angle. The initial and fin l particle spin projection quantum numbers are $m_p = \frac{1}{2}$, $m'_p = -\frac{1}{2}$, and $m_d = m'_d = 1$. Results for the CD Bonn + Δ two-baryon potential obtained with the screening radius $R = 5$ fm (black curves), 10 fm (blue curves), 15 fm (green curves), and 20 fm (red curves) are compared.

2.3 Renormalization in proton-deuteron scattering

For the nucleon-deuteron scattering it is convenient to consider nucleons as identical particles and use the isospin formalism. Since the isospin conservation is violated by the Coulomb force, both total $3N$ isospin $\mathcal{T} = \frac{1}{2}$ and $\frac{3}{2}$ states have to be included. The symmetrized transition operator for elastic scattering is the solution of the symmetrized AGS integral equation [19]

$$U^{(R)} = PG_0^{-1} + (1+P)u + PT^{(R)}G_0U^{(R)} + (1+P)uG_0(1+T^{(R)}G_0)U^{(R)}. \quad (37)$$

We omit the spectator index that is not needed anymore. The basis states are antisymmetric in the pair only, the full antisymmetry is ensured by $P = P_{12}P_{23} + P_{13}P_{23}$ where $P_{\alpha\beta}$ is the permutation operator of particles α and β. The breakup operator is then obtained from the quadrature

$$U_0^{(R)} = (1+P)[G_0^{-1} + u + T^{(R)}G_0U^{(R)} + uG_0(1+T^{(R)}G_0)U^{(R)}]. \quad (38)$$

The amplitudes for *p-d* elastic scattering and breakup referring to unscreened Coulomb are obtained after the renormalization of the corresponding on-shell matrix elements of the symmetrized transition operators, i.e.,

$$\langle \mathbf{q}'|U^{(C)}|\mathbf{q}\rangle = \langle \mathbf{q}'|T_C^{\rm c.m.}|\mathbf{q}\rangle + \lim_{R\to\infty}[Z_R^{-1}(q)\langle \mathbf{q}'|(U^{(R)} - T_R^{\rm c.m.})|\mathbf{q}\rangle], \quad (39)$$

$$\langle \mathbf{p}'\mathbf{q}'|U_0^{(C)}|\mathbf{q}\rangle = \lim_{R\to\infty}[z_R^{-\frac{1}{2}}(p')\langle \mathbf{p}'\mathbf{q}'|U_0^{(R)}|\mathbf{q}\rangle Z_R^{-\frac{1}{2}}(q)]. \quad (40)$$

However, a recent work [28] on an alternative Coulomb treatment in *pd* scattering proposed a different renormalization prescription: *p-d* elastic scattering amplitude calculated with screened Coulomb does not need renormalization at all, i.e., the limit $\lim_{R\to\infty}\langle \mathbf{q}'|U^{(R)}|\mathbf{q}\rangle$ should exist; the renormalization for the breakup amplitude is needed but it is different from ours given in Eq. (40). However, numerical results of Ref. [28] involve approximations that are not well under control. First, the screened Coulomb proton-proton transition matrix is approximated by the screened Coulomb potential thereby replacing a complex quantity by a real one. Second, the contributions $\langle \mathbf{q}'|PT_RPG_0T^{(R)}G_0U^{(R)}|\mathbf{q}\rangle$ and $\langle \mathbf{p}'\mathbf{q}'|(1+P)T_RPG_0T^{(R)}G_0U^{(R)}|\mathbf{q}\rangle$ to the elastic scattering

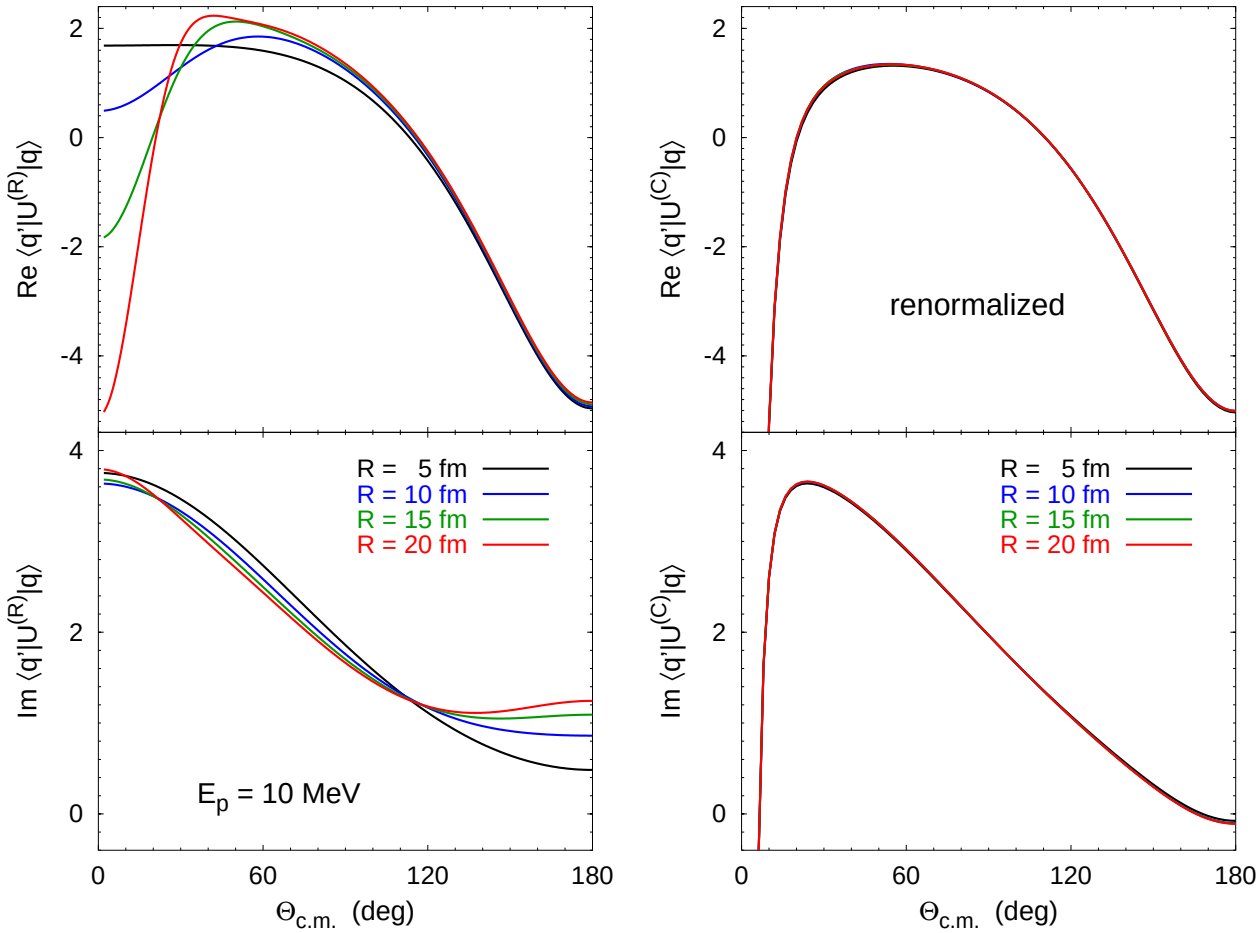

Fig. 4. Real and imaginary parts of nonrenormalized (left side) and renormalized (right side) *p-d* elastic scattering amplitudes (in arbitrary units) at $E_p = 10$ MeV shown as functions of the c.m. scattering angle. The initial and fin l particle spin projection quantum numbers are $m_p = m'_p = \frac{1}{2}$, and $m_d = m'_d = 1$. Curves as in Fig. 3.

and breakup amplitudes, respectively, are neglected; this may have even more serious consequences since the above terms among others include screened Coulomb contributions that are of the leading (first order. Indeed, under the approximations of Ref. [28] the R-dependence of the resulting screened Coulomb amplitude for *p-d* elastic scattering is weak and the $R \to \infty$ limit of renormalized amplitude in Eq. (39) does not exists. However, the situation changes completely when the scattering amplitudes are calculated exactly as in our work. In Figs. 3 and 4 we study the dependence on the screening radius R for selected components of the nonrenormalized and renormalized *p-d* elastic scattering amplitudes $\langle \mathbf{q}'|U^{(R)}|\mathbf{q}\rangle$ and $\langle \mathbf{q}'|U^{(C)}|\mathbf{q}\rangle$. The CD Bonn + Δ two-baryon potential [29] is taken as the hadronic interaction and the proton lab energy $E_p = 10$ MeV. In Fig. 3 we show spin-nondiagonal amplitudes that have only the Coulomb-distorted short-range part. The nonrenormalized amplitude $\langle \mathbf{q}'|U^{(R)}|\mathbf{q}\rangle$ shows a clear R-dependence; in fact, its absolute value becomes R-independent but the phase changes like $\ln R$. In contrast, the renormalized amplitude $\langle \mathbf{q}'|U^{(C)}|\mathbf{q}\rangle$, within the accuracy of the plot, becomes independent of R for $R \geq 10$ fm. The spin-diagonal amplitude having also a long-range part shows, as expected, very strong R-dependence at small scattering angles before renormalization but becomes R-independent after renormalization as well as Fig. 4 demonstrates. In Fig. 5 we show the corresponding results for *p-d* breakup at $E_p = 13$ MeV in the space star configu ration. For breakup reaction the renormalized amplitude $\langle \mathbf{p}'\mathbf{q}'|U_0^{(C)}|\mathbf{q}\rangle$ converges with the screening radius somehow slower than for elastic scattering, it becomes independent of R for $R \geq 20$ fm whereas the nonrenormalized amplitude $\langle \mathbf{p}'\mathbf{q}'|U_0^{(R)}|\mathbf{q}\rangle$ shows a clear R-dependence. Furthermore, although the breakup amplitude (without the three-nucleon force) can be decomposed into three terms $T_\gamma^{(R)} G_0 U_{\gamma\alpha}^{(R)}$, separately none of them has an $R \to \infty$ limit with or without renormalization in contrast to the conjecture of Ref. [28]; infinit R limit exists only for renormalized full breakup amplitude. Thus, fully converged numerical results without uncontrolled approximations clearly support the standard screening and renormalization theory as given in Eqs. (39) and (40) and not the one of Ref. [28].

The convergence of the observables with the screening radius R used to calculate the Coulomb-distorted short-range part of the amplitudes is the internal criterion for

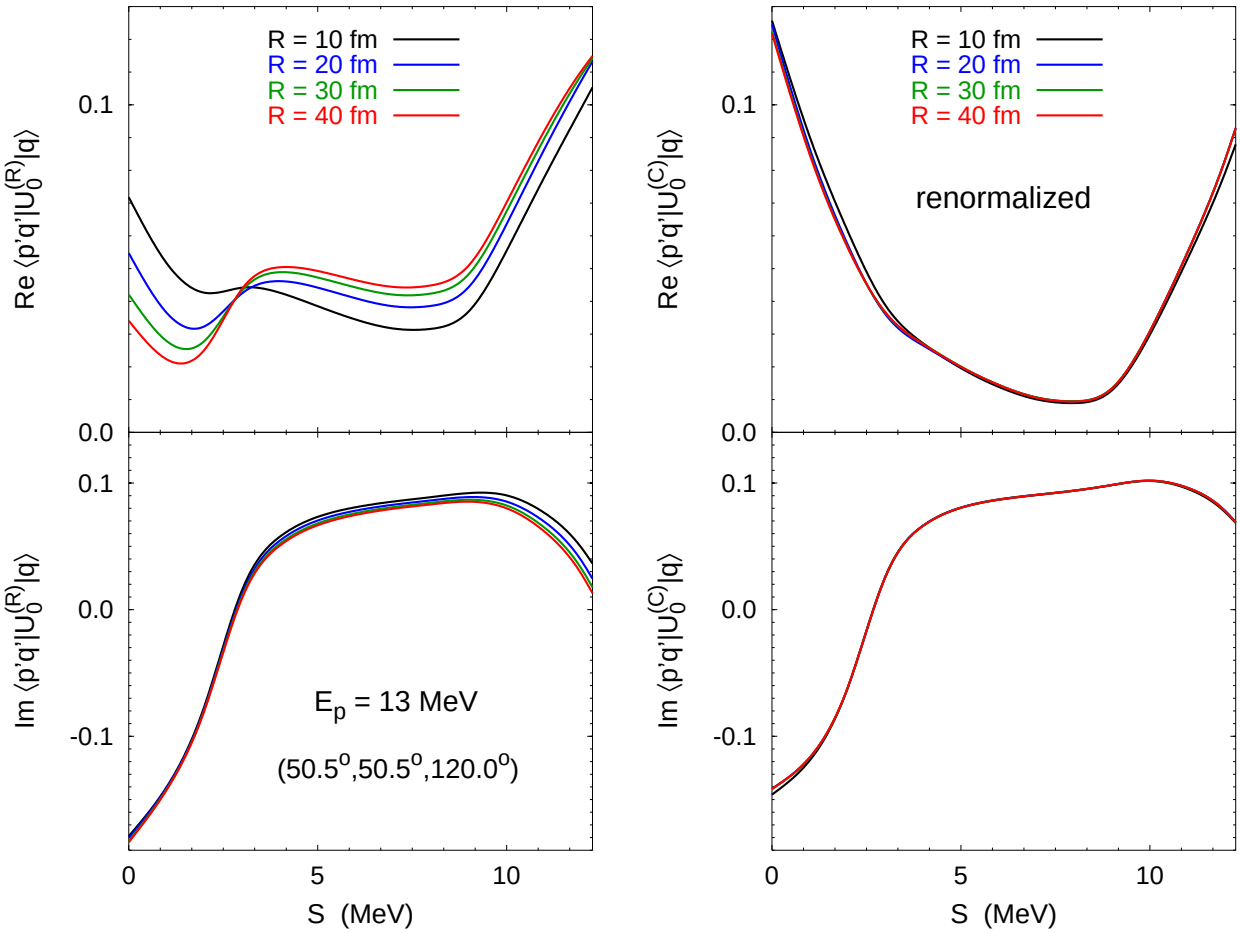

Fig. 5. Real and imaginary parts of nonrenormalized (left side) and renormalized by $\exp\{i[\kappa(p) + \mathcal{K}(q)] \ln R\}$ (right side) *p-d* breakup amplitudes (in arbitrary units) at $E_p = 13$ MeV in the space star configuratio shown as functions of the arclength S along the kinematical curve. Curves as in Fig. 3.

the reliability of our method. Numerous examples can be found in Refs. [12,13,30,31]. In most cases the convergence is impressively fast; the screening radius $R = 10$ to 30 fm is sufficient. The exceptions requiring larger screening radii are the observables at very low energies and the breakup differential cross section in kinematical situations characterized by very low relative energy $E_{\rm rel}$ between the two charged particles, e.g., *p-d* breakup or photodisintegration of ^{3}He close to the *pp* final-stat interaction (*pp*-FSI) regime [13]. The slow convergence under those conditions is not surprising, since the renormalization factor itself as well as the Coulomb parameter become ill-defined indicating that the screening and renormalization procedure cannot be applied at $E_{\rm rel} = 0$. Therefore an extrapolation has to be used to calculate the observables at $E_{\rm rel} = 0$, which works pretty well when the observables vary smoothly with $E_{\rm rel}$ which is the case in three-body breakup reactions. Furthermore, the results for *p-d* elastic scattering obtained by the present technique were compared [32] with those of Ref. [9] obtained from the variational solution of the three-nucleon Schrödinger equation in configuratio space with the inclusion of an *unscreened* Coulomb potential between the protons and imposing the proper Coulomb boundary conditions explicitly. Good agreement over a wide energy range was found indicating that both techniques for including the Coulomb interaction are reliable. At very low energies the coordinate-space treatments remain favored since there the method of screening and renormalization converges slowly and therefore becomes technically too demanding, but at higher energies and for three-body breakup reactions it is more efficient.

3 Results

In this section we present selected results for reactions in various three- and four-body nuclear systems.

3.1 Proton-deuteron scattering

Realistic models for the nuclear interaction are used, e.g., CD Bonn +Δ two-baryon potential [29] yielding an effective three-nucleon force or the AV18 two-nucleon potential [37] with the irreducible Urbana IX (UIX) three-nucleon

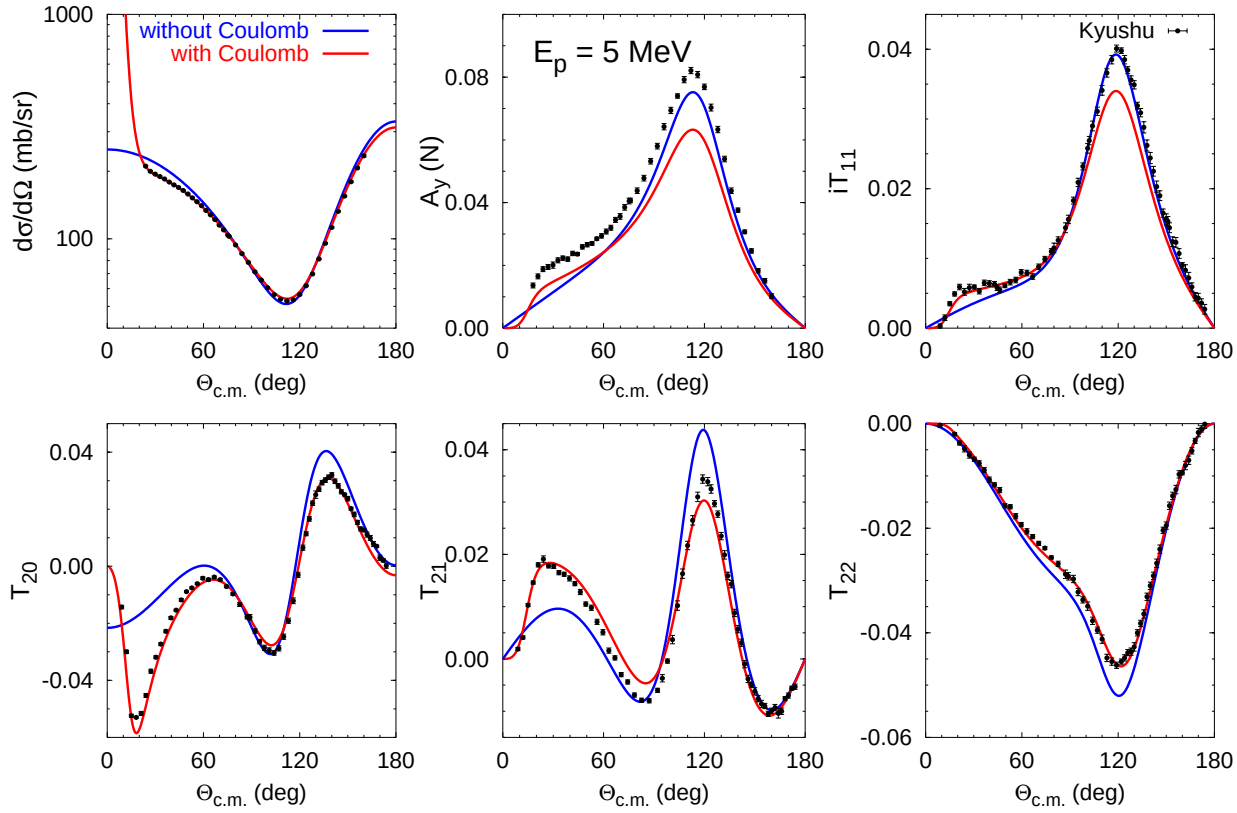

Fig. 6. Differential cross section and analyzing powers for *p-d* elastic scattering at 5 MeV proton lab energy as functions of the c.m. scattering angle. Results including the Coulomb interaction (red curves) are compared to results without Coulomb (blue curves). Hadronic potential is CD Bonn + Δ. The experimental data are from Ref. [33].

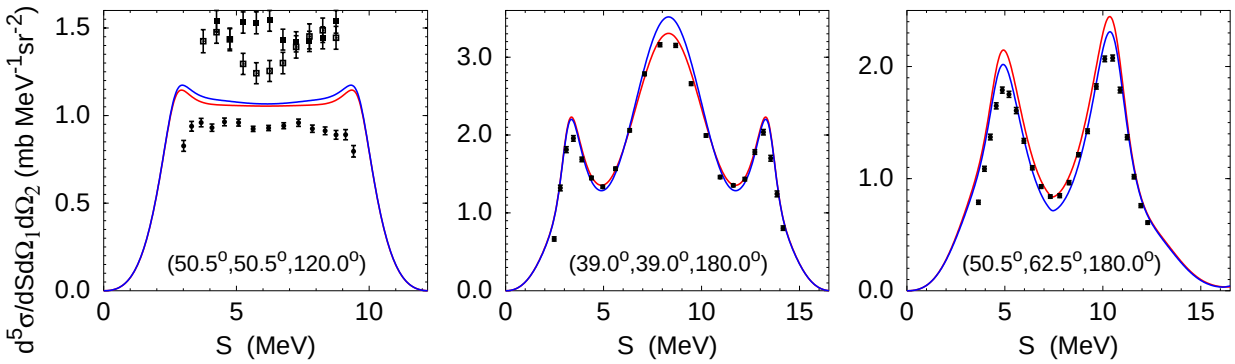

Fig. 7. Differential cross section for *p-d* breakup at 13 MeV proton lab energy in space star (left), quasifree scattering (middle), and collinear (right) configurations as function of the arclength S along the kinematical curve. Results including the Coulomb interaction (red curves) are compared to results without Coulomb (blue curves). Hadronic interaction model is AV18 + UIX. The experimental data are from Ref. [34] (full circles). For the space star configuration also the *nd* data from Refs. [35, 36] (open and full squares) are shown.

force [38]. The Coulomb effect is important in low-energy *p-d* elastic scattering as Fig. 6 demonstrates; the description of the experimental data is quite satisfactory except for the proton and deuteron vector analyzing powers. In *p-d* elastic scattering at higher energies the Coulomb effect gets confined to forward angles.

In Fig. 7 we show results for *p-d* breakup at 13 MeV proton lab energy. Although the inclusion of the Coulomb force slightly improves the agreement with data in the space star configuration, the Coulomb effect is far too small to reproduce the difference between the experimental *p-d* and *n-d* data and to resolve the so-called *space star anomaly*. Slightly larger and beneficial Coulomb effects are seen in quasifree scattering (QFS) and collinear configurations.

The Coulomb effect in may become large even at higher energies when the relative *pp* energy in the final state is very low as demonstrated in Fig. 8 for *p-d* breakup at 130 MeV deuteron lab energy. In there, the Coulomb repulsion

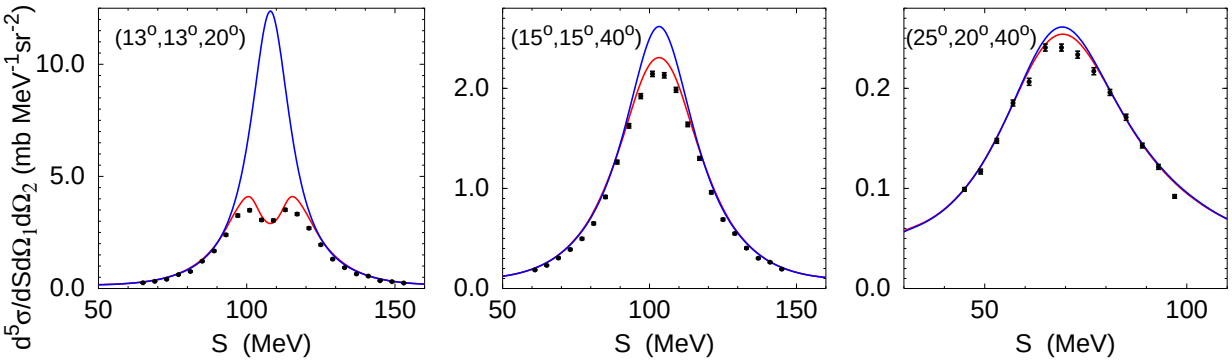

Fig. 8. Differential cross section for *pd* breakup at 130 MeV deuteron lab energy in selected kinematical configurations with small relative azimuthal angle. Curves as in Fig. 7 and the experimental data from Refs. [39, 40].

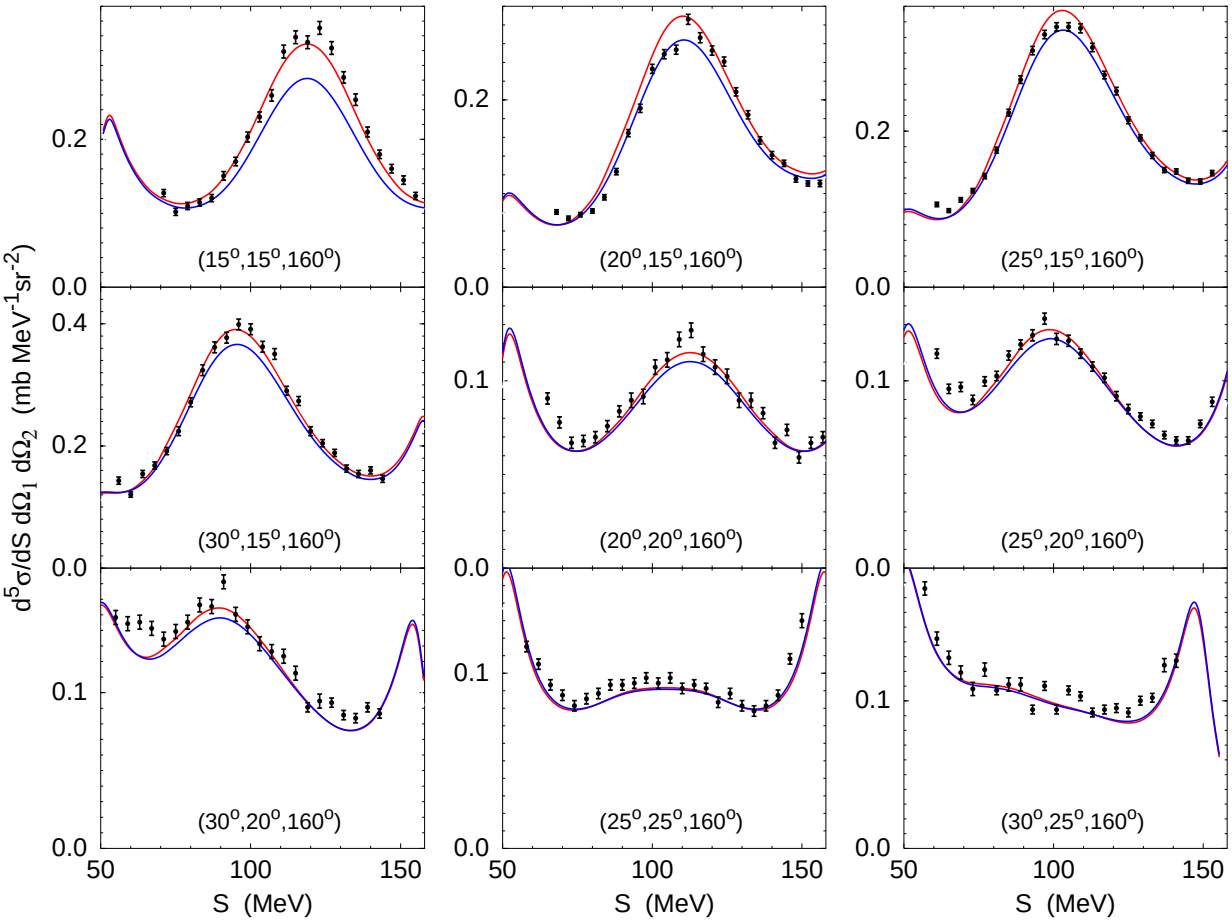

Fig. 9. Differential cross section for *p-d* breakup at 130 MeV deuteron lab energy in selected kinematical configurations with large relative azimuthal angle. Curves as in Fig. 7 and the experimental data from Ref. [39].

is responsible for decreasing the cross section; the *pp*-FSI peak obtained in the absence of Coulomb may even be converted into a minimum. However, in some other configurations Coulomb may lead to a moderate increase of the differential cross section as shown in Fig. 9.

3.2 Photodisintegration of ^{3}He

The results are obtained with the CD Bonn +Δ two-baryon potential and include effective two- and three-nucleon electromagnetic currents mediated by the Δ isobar [41, 42]. As in *p-d* breakup, the Coulomb effect may be very strong in the three-body photodisintegration of ^{3}He close to the *pp*-FSI kinematics. The effect remains also after partial integration when calculating the semi-inclusive observables

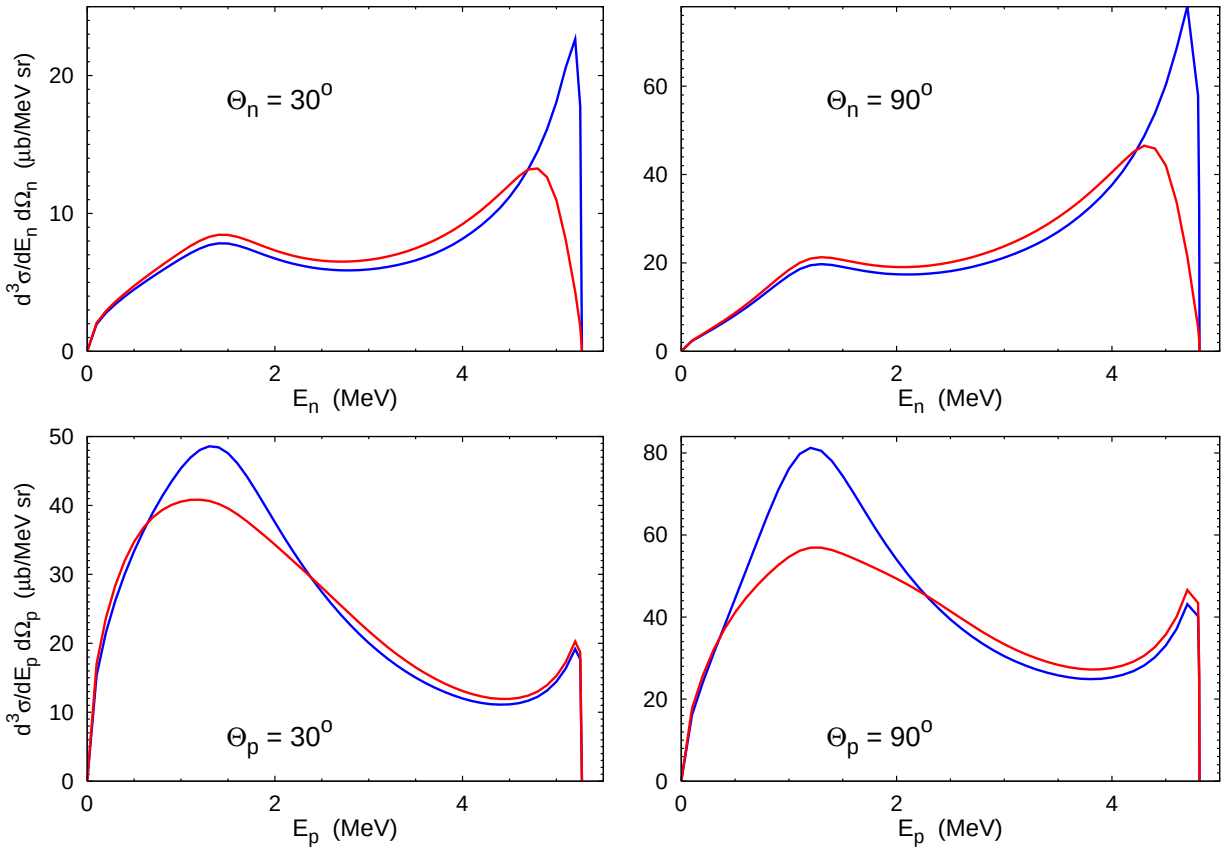

Fig. 10. The semi-inclusive threefold differential cross section for the ^{3}He$(\gamma, n)pp$ (top) and ^{3}He$(\gamma, p)pn$ (bottom) reactions at 15 MeV photon lab energy as function of the detected nucleon energy at 30° and 90° nucleon scattering angles. Curves as in Fig. 6.

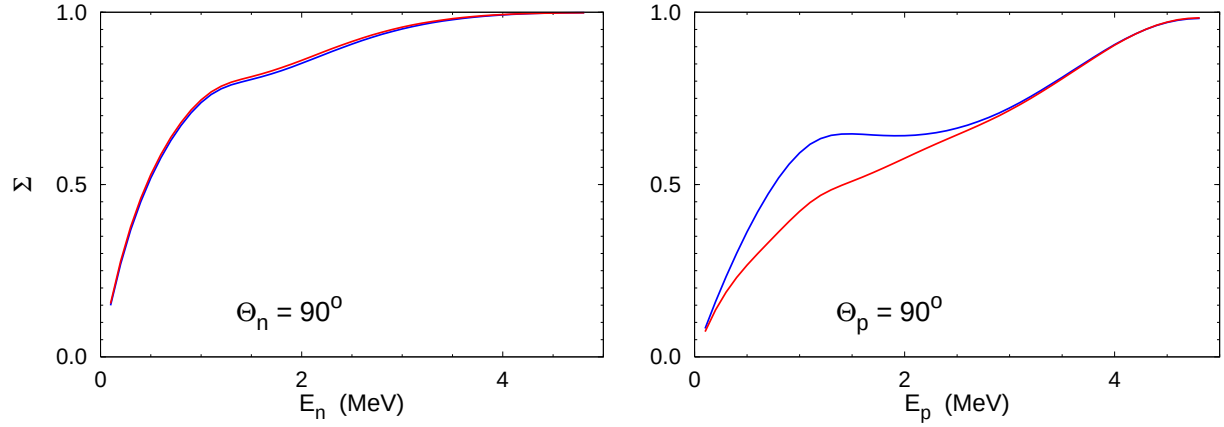

Fig. 11. The semi-inclusive linear photon asymmetry for the ^{3}He$(\gamma, n)pp$ (left) and ^{3}He$(\gamma, p)pn$ (right) reactions at 15 MeV photon lab energy as function of the detected nucleon energy at 90° nucleon scattering angle. Curves as in Fig. 6.

as shown in Figs. 10 and 11. Not only the differential cross section gets affected but also the spin observables like the linear photon asymmetry for ^{3}He$(\gamma, p)pn$ reaction.

3.3 Three-body nuclear reactions

The screening and renormalization method in the framework of momentum-space AGS equations can be applied to the description of three-body-like nuclear reactions involving heavier nuclei whose interaction with nucleons is described by the optical potentials. Examples are deuteron scattering on a stable nucleus A or proton scattering on a

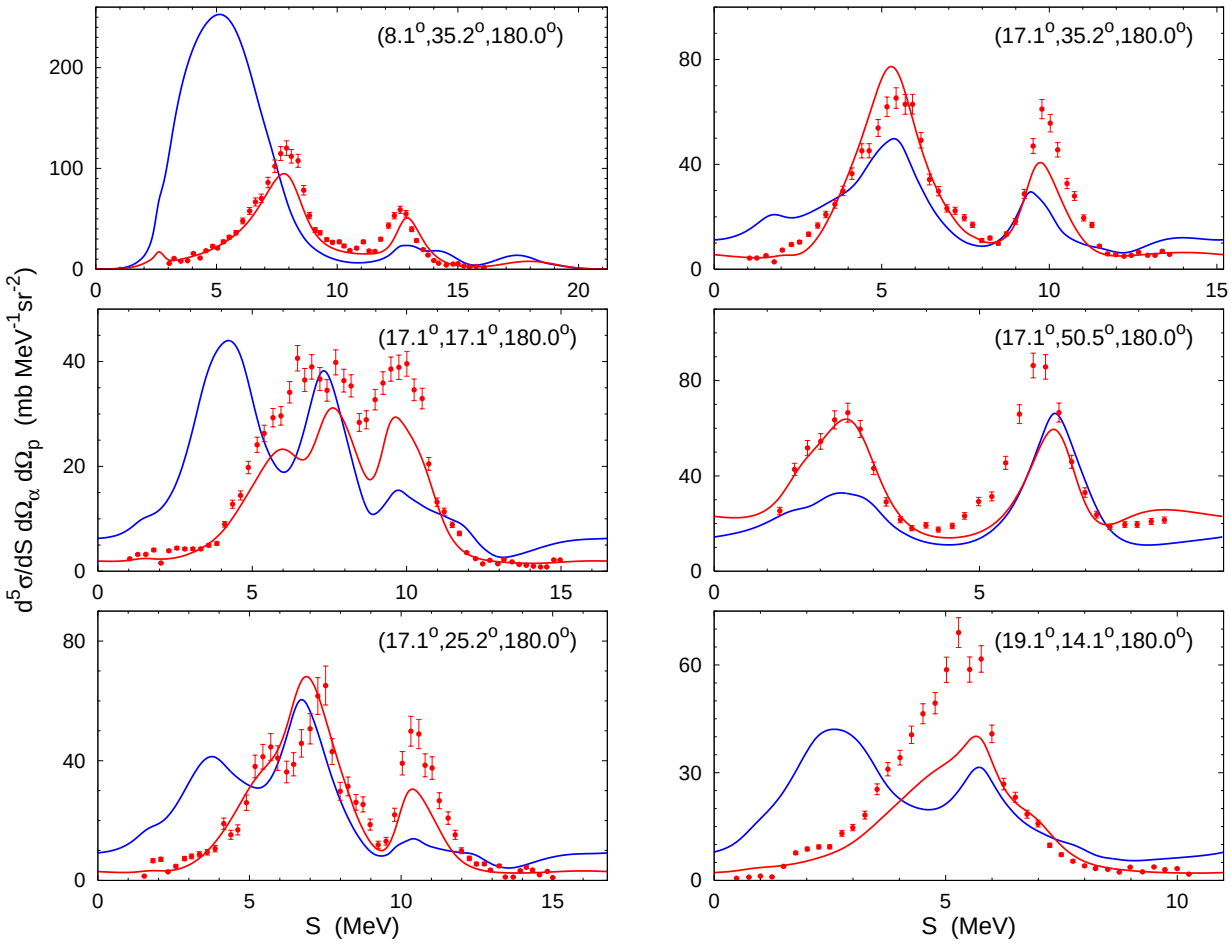

Fig. 12. Differential cross section for α-d breakup at 15 MeV α lab energy in selected kinematical configurations as function of the arclength S along the kinematical curve. Results including the Coulomb interaction (red curves) are compared to results without Coulomb (blue curves). The experimental data are from Ref. [43].

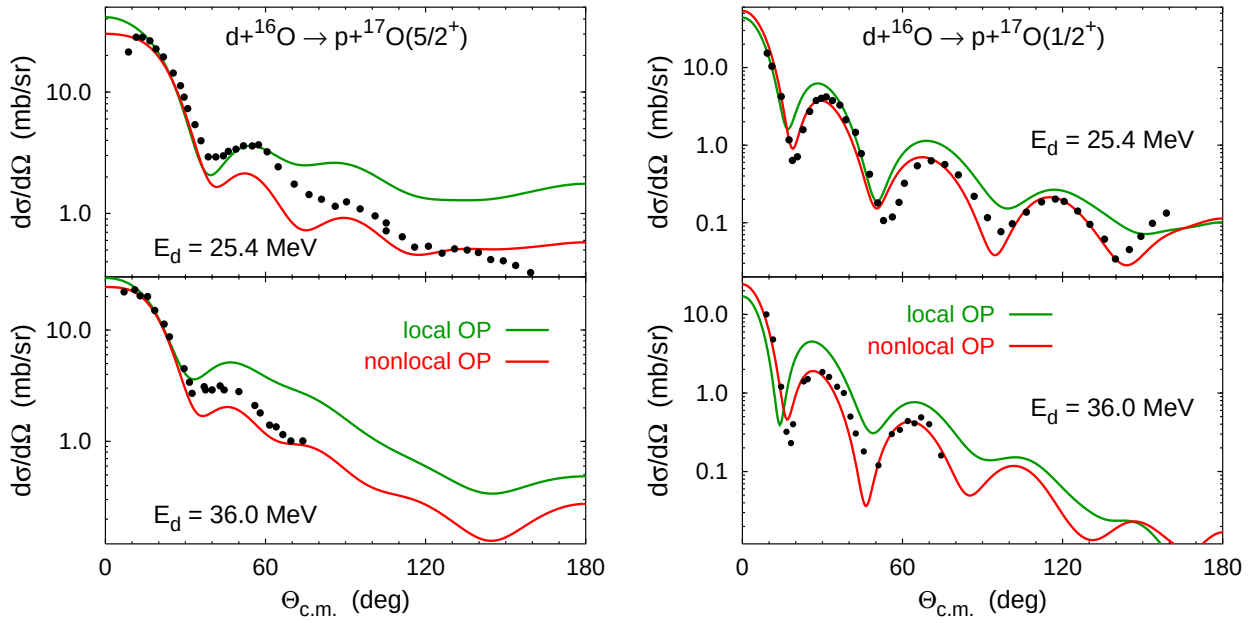

Fig. 13. Differential cross section for $d + {}^{16}\mathrm{O} \rightarrow p + {}^{17}\mathrm{O}$ transfer to the ${}^{17}\mathrm{O}$ ground state $5/2^+$ (left side) and excited state $1/2^+$ (right side) at E_d = 25.4 and 36.0 MeV calculated with local and nonlocal optical potentials. The experimental data are from Ref. [44].

weakly bound two-body system (An) consisting of the core A and the neutron n; all elastic, transfer, charge-exchange, and breakup reactions, allowed by the chosen Hamiltonian, can be calculated on the same footing. The calculations have been performed for a number of reactions with the core A ranging from the α particle to ^{58}Ni [30,45,46].

In Fig. 12 we show the differential cross section for α-d breakup reaction at 15 MeV α lab energy that is calculated using three-body (α, p, n) model. The most important Coulomb effect is the shift of the αp P-wave resonance position that leads to the corresponding changes in the structure of the observables. The predictions without Coulomb fail completely in accounting for the experimental data, while inclusion of the Coulomb moves the peaks of the differential cross section to the right positions, although the height of those peaks is not always reproduced, probably due to deficiencie of the nucleon-α potentials.

The developed technique allowed to test the accuracy of traditional approximate nuclear reaction approaches like Continuum Discretized Coupled Channels (CDCC) method [47] as has been done in Ref. [48] for d + ^{12}C, d + ^{58}Ni, and $p+^{11}$Be reactions. It was found that CDCC is indeed a reliable method to calculate $d+A$ elastic and breakup cross sections but may lack accuracy for transfer reactions such as $p+^{11}\mathrm{Be} \rightarrow d+^{10}\mathrm{Be}$ and for breakup of one-neutron halo nuclei p + ^{11}Be $\rightarrow$ $p + n$ + ^{10}Be. Furthermore, novel dynamical input like energy-dependent [49] or nonlocal optical potentials [50,51] could be included for the firs time due to the use of the momentum-space framework. Especially important nonlocality effects were found for (d, p) and (p, d) transfer reactions involving stable [52] as well as exotic nuclei [53].

3.4 Four-nucleon scattering

Exact description of the four-nucleon scattering is given by the Faddeev-Yakubovsky equations [54] for the wave-function components or by the equivalent AGS equations [55]. We use isospin formalism and solve the symmetrized AGS equations [56] for the transition operators. Coulomb interaction is included using the same idea of screening and renormalization. Long- and Coulomb-distorted short-range parts in the scattering amplitudes are separated [57, 58]. The former is of two-body nature and its $R \rightarrow \infty$ limit is known analytically. The Coulomb-distorted short-range part is calculated by solving symmetrized AGS equations numerically where the screened Coulomb potential is added to the nuclear proton-proton potential; the $R \rightarrow \infty$ limit is reached with sufficient accuracy at finit screening radii R as demonstrated in Ref. [57].

The four-nucleon scattering calculations have been performed so far only below three-body breakup threshold where the Coulomb effect is extremely important. This is demonstrated in Fig. 14 for proton-^{3}He elastic scattering at 4 MeV proton lab energy. As in p-d scattering, the proton analyzing power is underpredicted by the theory [57,59].

In Figs. 15 and 16 we show examples for transfer and charge-exchange reactions in the four-nucleon system. The two-nucleon interactions we use are AV18 [37], the one derived from chiral perturbation theory at next-to-next-to-next-to-leading order (N3LO) [62], CD Bonn [63], and inside nonlocal outside Yukawa (INOY04) potential by Doleschall [64]. Although here we do not include a three-nucleon force, its presence is simulated by using the potential INOY04 that fit both ^{3}He and ^{3}H experimental binding energies (7.72 MeV and 8.48 MeV, respectively). The results for the two-baryon potential CD Bonn + Δ [29] allowing for a virtual excitation of a nucleon to a Δ-isobar and thereby yielding consistent effective three- and four-nucleon forces are qualitatively similar and can be found in Ref. [65]. Most of the experimental data are quite well described [57–59,66] at least by some of the used two-nucleon force models, but there exist also several discrepancies, e.g., for the neutron-^{3}H total cross section [56,67] and for the proton analyzing power in the proton-^{3}He elastic scattering [57,59,60] and in the p + ^{3}H $\rightarrow$ n + ^{3}He charge-exchange reaction [58].

4 Summary

We used the method of screening and renormalization to include the Coulomb interaction between the charged particles in few-body nuclear reactions. We demonstrated analytically and numerically that the limit of infinit screening radius exists only for renormalized amplitudes. The short range part of the scattering amplitudes were obtained from the exact few-body scattering equations that were solved in the momentum-space framework. We obtained fully converged results for three- and four-nucleon scattering and for three-body-like nuclear reactions.

References

1. A. Kievsky, S. Rosati, W. Tornow, M. Viviani, Nucl. Phys. **A607**, 402 (1996)
2. C.R. Chen, J.L. Friar, G.L. Payne, Few-Body Syst. **31**, 13 (2001)
3. S. Ishikawa, Few-Body Syst. **32**, 229 (2003)
4. P. Doleschall, Z. Papp, Phys. Rev. **C72**, 044003 (2005)
5. E.O. Alt, S.B. Levin, S.L. Yakovlev, Phys. Rev. **C69**, 034002 (2004)
6. A.S. Kadyrov, I. Bray, A.M. Mukhamedzhanov, A.T. Stelbovics, Phys. Rev. A **72**, 032712 (2005)
7. A.S. Kadyrov, I. Bray, A.M. Mukhamedzhanov, A.T. Stelbovics, Ann. Phys. **324**, 1516 (2005)
8. S. Oryu, Phys. Rev. **C73**, 054001 (2006)
9. A. Kievsky, M. Viviani, S. Rosati, Phys. Rev. **C64**, 024002 (2001)
10. E.O. Alt, M. Rauh, Few-Body Syst. **17**, 121 (1994)
11. E.O. Alt, A.M. Mukhamedzhanov, M.M. Nishonov, A.I. Sattarov, Phys. Rev. C **65**, 064613 (2002)
12. A. Deltuva, A.C. Fonseca, P.U. Sauer, Phys. Rev. **C71**, 054005 (2005)
13. A. Deltuva, A.C. Fonseca, P.U. Sauer, Phys. Rev. **C72**, 054004 (2005)
14. S. Ishikawa, Phys. Rev. **C80**, 054002 (2009)
15. J.R. Taylor, Nuovo Cimento B **23**, 313 (1974)

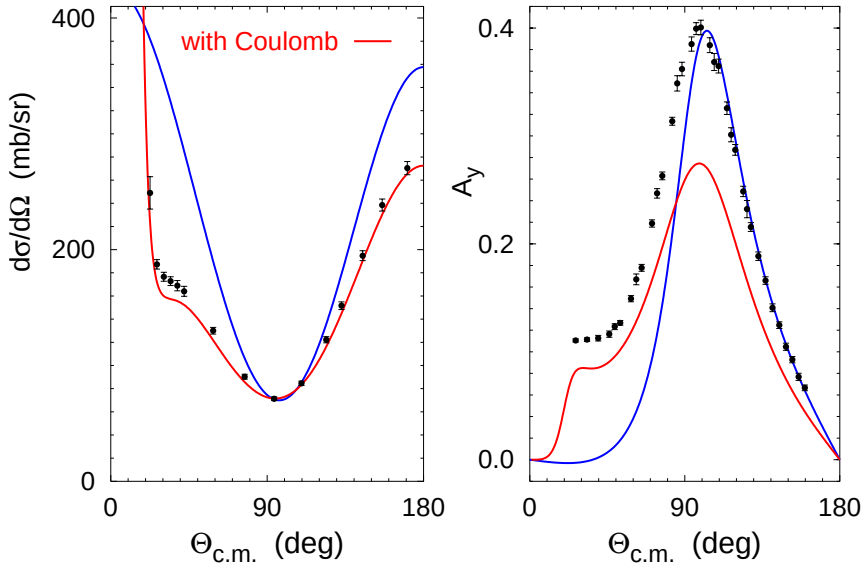

Fig. 14. Differential cross section and proton analyzing power for p-^{3}He elastic scattering at 4 MeV proton lab energy as functions of the c.m. scattering angle. Results including the Coulomb interaction (red curves) are compared to results without Coulomb (blue curves). Hadronic potential is CD Bonn. The experimental data are from Refs. [60,61].

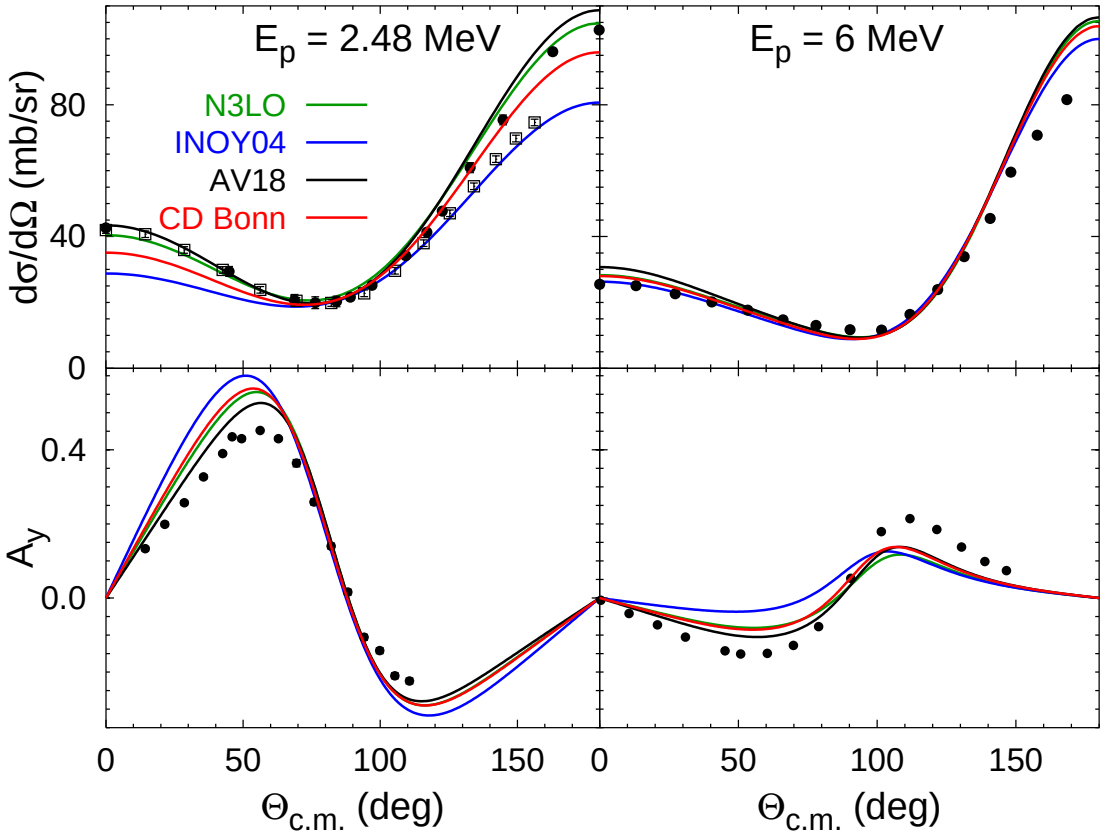

Fig. 15. Differential cross section and proton analyzing power of $p + {}^3\mathrm{H} \rightarrow n + {}^3\mathrm{He}$ reaction at 2.48 and 6 MeV proton lab energy calculated with various realistic two-nucleon potentials. The cross section data are from Refs. [68] (circles) and [69] (squares) at 2.48 MeV, and from Ref. [70] at 6 MeV. A_y data are from Ref. [71] at 2.48 MeV and from Ref. [72] at 6 MeV.

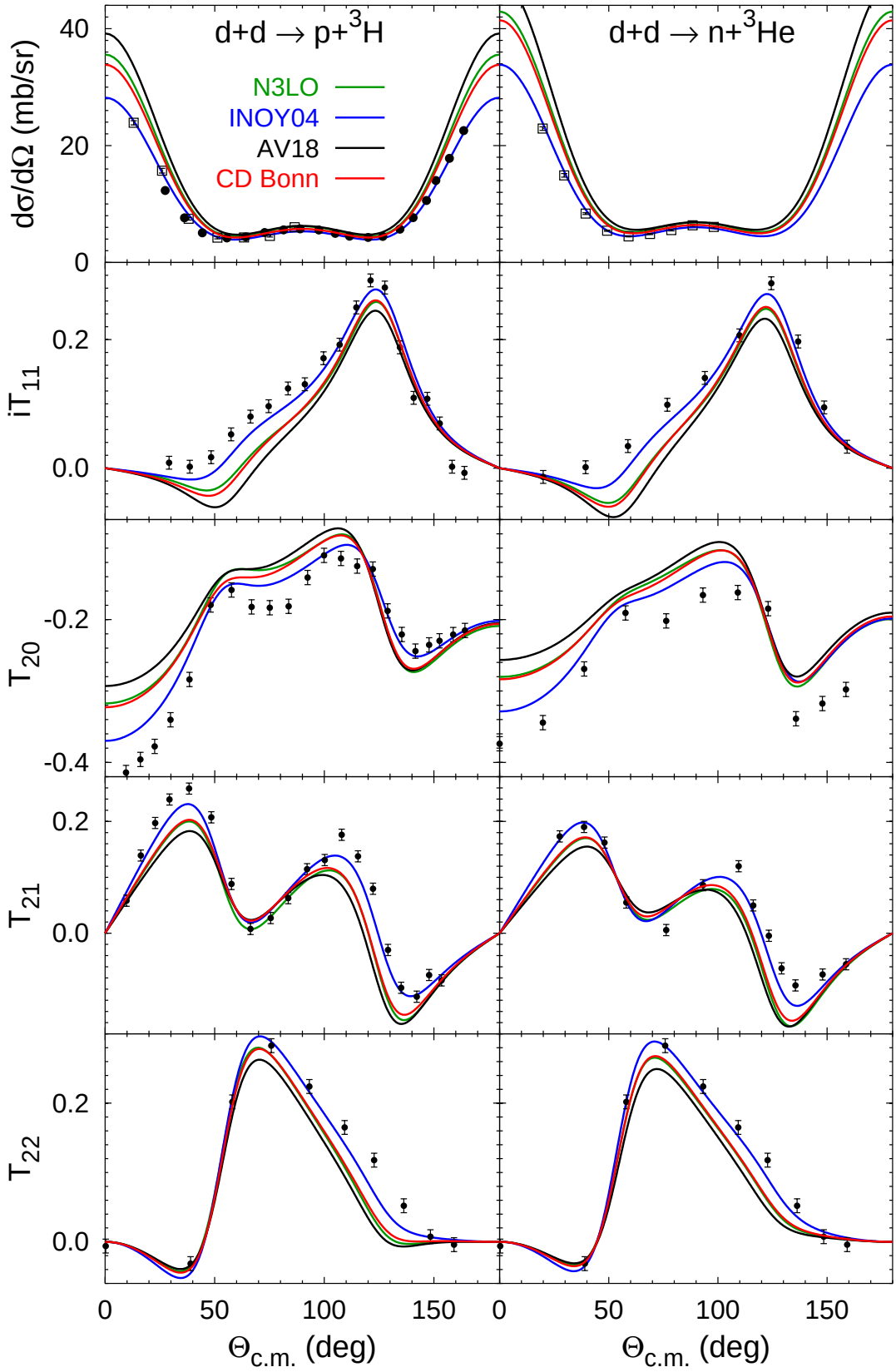

Fig. 16. Differential cross section and deuteron analyzing powers of $d + d \rightarrow p + {}^3\mathrm{H}$ and $d + d \rightarrow n + {}^3\mathrm{He}$ reactions at 3 MeV deuteron lab energy. The cross section data are from Refs. [73] (squares) and [74] (circles) and the analyzing power data are from Refs. [74, 75].

16. M.D. Semon, J.R. Taylor, Nuovo Cimento A **26**, 48 (1975)
17. V.G. Gorshkov, Sov. Phys.-JETP **13**, 1037 (1961)
18. A. Deltuva, A.C. Fonseca, P.U. Sauer, Annu. Rev. Nucl. Part. Sci. **58**, 27 (2008)
19. A. Deltuva, Phys. Rev. **C80**, 064002 (2009)
20. E.O. Alt, P. Grassberger, W. Sandhas, Nucl. Phys. **B2**, 167 (1967)
21. K. Chmielewski, A. Deltuva, A.C. Fonseca, S. Nemoto, P.U. Sauer, Phys. Rev. C **67**, 014002 (2003)
22. A. Deltuva, K. Chmielewski, P.U. Sauer, Phys. Rev. **C67**, 034001 (2003)
23. A. Deltuva, Ph.D. thesis, University of Hannover (2003), http://edok01.tib.uni-hannover.de/edoks/e01dh03/374454701.pdf
24. G.H. Berthold, A. Stadler, H. Zankel, Phys. Rev. **C41**, 1365 (1990)
25. E.O. Alt, A.M. Mukhamedzhanov, A.I. Sattarov, Phys. Rev. Lett. **81**, 4820 (1998)
26. A. Deltuva, K. Chmielewski, P.U. Sauer, Phys. Rev. **C67**, 054004 (2003)
27. A. Deltuva, A.C. Fonseca, P.U. Sauer, Phys. Rev. **C73**, 057001 (2006)
28. H. Witała, R. Skibinski, J. Golak, W. Glöckle, Eur. Phys. J. **A41**, 369 (2009); **A41**, 385 (2009)
29. A. Deltuva, R. Machleidt, P.U. Sauer, Phys. Rev. **C68**, 024005 (2003)
30. A. Deltuva, Phys. Rev. **C74**, 064001 (2006)
31. A. Deltuva, A.C. Fonseca, P.U. Sauer, Nucl. Phys. **A790**, 52c (2007)
32. A. Deltuva, A.C. Fonseca, A. Kievsky, S. Rosati, P.U. Sauer, M. Viviani, Phys. Rev. **C71**, 064003 (2005)
33. K. Sagara, H. Oguri, S. Shimizu, K. Maeda, H. Nakamura, T. Nakashima, S. Morinobu, Phys. Rev. **C50**, 576 (1994)
34. G. Rauprich, S. Lemaitre, P. Niessen, K.R. Nyga, R. Reckenfelderbäumer, L. Sydow, H. Paetz gen. Schieck, H. Witała, W. Glöckle, Nucl. Phys. **A535**, 313 (1991)
35. J. Strate *et al.*, Nucl. Phys. **A501**, 51 (1989)
36. H.R. Setze *et al.*, Phys. Rev. **C71**, 034006 (2005)
37. R.B. Wiringa, V.G.J. Stoks, R. Schiavilla, Phys. Rev. **C51**, 38 (1995)
38. B.S. Pudliner, V.R. Pandharipande, J. Carlson, S.C. Pieper, R.B. Wiringa, Phys. Rev. **C56**, 1720 (1997)
39. S. Kistryn *et al.*, Phys. Rev. **C72**, 044006 (2005)
40. S. Kistryn *et al.*, Phys. Lett. B **641**, 23 (2006)
41. A. Deltuva, L.P. Yuan, J. Adam Jr., A.C. Fonseca, P.U. Sauer, Phys. Rev. C **69**, 034004 (2004)
42. A. Deltuva, L.P. Yuan, J. Adam Jr., P.U. Sauer, Phys. Rev. **C70**, 034004 (2004)
43. I. Koersner, L. Glantz, A. Johansson, B. Sundqvist, H. Nakamura, H. Noya, Nucl. Phys. **A286**, 431 (1977)
44. M.D. Cooper, W.F. Hornyak, P.G. Roos, Nucl. Phys. **A218**, 249 (1974)
45. A. Deltuva, Nucl. Phys. **A821**, 72 (2009)
46. E. Cravo, R. Crespo, A. Deltuva, A.C. Fonseca, Phys. Rev. **C79**, 064610 (2009)
47. N. Austern, Y. Iseri, M. Kamimura, M. Kawai, G. Rawitscher, M. Yahiro, Phys. Rep. **154**, 125 (1987)
48. A. Deltuva, A.M. Moro, E. Cravo, F.M. Nunes, A.C. Fonseca, Phys. Rev. C **76**, 064602 (2007)
49. A. Deltuva, A.C. Fonseca, Phys. Rev. **C79**, 014606 (2009)
50. M.M. Giannini, G. Ricco, Ann. Phys. (NY) **102**, 458 (1976)
51. M.M. Giannini, G. Ricco, A. Zucchiatti, Ann. Phys. (NY) **124**, 208 (1980)
52. A. Deltuva, Phys. Rev. **C79**, 021602 (2009)
53. A. Deltuva, Phys. Rev. **C79**, 054603 (2009)
54. O.A. Yakubovsky, Yad. Fiz. **5**, 1312 (1967) [Sov. J. Nucl. Phys. **5**, 937 (1967)]
55. P. Grassberger, W. Sandhas, Nucl. Phys. **B2**, 181 (1967); E. O. Alt, P. Grassberger, and W. Sandhas, JINR report No. E4-6688 (1972)
56. A. Deltuva, A.C. Fonseca, Phys. Rev. **C75**, 014005 (2007)
57. A. Deltuva, A.C. Fonseca, Phys. Rev. Lett. **98**, 162502 (2007)
58. A. Deltuva, A.C. Fonseca, Phys. Rev. **C76**, 021001 (2007)
59. M. Viviani, A. Kievsky, S. Rosati, E.A. George, L.D. Knutson, Phys. Rev. Lett. **86**, 3739 (2001)
60. B.M. Fisher, C.R. Brune, H.J. Karwowski, D.S. Leonard, E.J. Ludwig, T.C. Black, M. Viviani, A. Kievsky, S. Rosati, Phys. Rev. **C74**, 034001 (2006)
61. M.T. Alley, L.D. Knutson, Phys. Rev. **C48**, 1890 (1993)
62. D.R. Entem, R. Machleidt, Phys. Rev. **C68**, 041001(R) (2003)
63. R. Machleidt, Phys. Rev. **C63**, 024001 (2001)
64. P. Doleschall, Phys. Rev. **C69**, 054001 (2004)
65. A. Deltuva, A.C. Fonseca, P.U. Sauer, Phys. Lett. **B660**, 471 (2008)
66. R. Lazauskas, Phys. Rev. **C79**, 054007 (2009)
67. R. Lazauskas, J. Carbonell, Phys. Rev. **C70**, 044002 (2004)
68. M. Drosg, Nucl. Sci. Eng. **67**, 190 (1978)
69. G.A. Jarvis, Los Alamos Scientifi Lab Reports No. **2014**, 35 (1956)
70. W.E. Wilson, R.L. Walter, D.B. Fossan, Nucl. Phys. **27**, 421 (1961)
71. M.A. Doyle, H.W. Clark, L.J. Dries, J.L. Regner, T.R. Donoghue, G.M. Hale, Nucl. Phys. **A371**, 225 (1981)
72. J.J. Jarmer, R.C. Haight, J.E. Simmons, J.C. Martin, T.R. Donoghue, Phys. Rev. **C9**, 1292 (1974)
73. J.M. Blair, G. Freier, E. Lampi, W. Sleator, J.H. Williams, Phys. Rev. **74**, 1599 (1948)
74. W. Grüebler, V. König, P.A. Schmelzbach, R. Risler, R.E. White, P. Marmier, Nucl. Phys. **A193**, 129 (1972)
75. L.J. Dries, H.W. Clark, R. Detomo, T.R. Donoghue, Phys. Lett. **80B**, 176 (1979)